This is the final version of this paper after peer review but before formal typesetting.
The published version is available at **DOI:**10.3233/SFC-228004
Strength, Fracture and Complexity, vol. 15, no. 1, pp. 47-57, 2022, or at this link:
https://content.iospress.com/articles/strength-fracture-and-complexity/sfc228004

UNDERSTANDING SIGNAL CHANGES WHEN MONITORING CREEP DAMAGE IN HIGH TEMPERATURE PLANT USING DCPD

A Wojcik, Department of Mechanical Engineering, University College London, UK
a.wojcik@ucl.ac.uk
A S Santos, M Waitt, Matelect Ltd, Harefield, UK
A Shibli, ETD Ltd, Leatherhead, UK

Abstract

The electrical potential drop (EPD) technique has previously shown promising results using a combination of AC and DC EPD (or DCPD) on large pressure vessel creep tests, detecting final cracking as well as incipient creep cavitation damage in welded P91 steel, with DCPD showing subtle but steady rises of around 5% over ca 10,000hrs of testing before rising exponentially at failure. The work presented here has attempted to shed light upon this using a simple numerical model. The model uses an array of spherical cavities to constrain the current path and hence raise the DCPD, however it was only able to show a modest rise in DCPD, and not match experimentally determined rises. Modelled DCPD values were a fifth of those experimentally observed, but both the nature of the model (simplified to aid timely computation) and the assumption that only cavitation is responsible for the changes seen, could be the reason for the discrepancies reported here. The possibility remains that other mechanisms are at play, which could magnify the measured DCPD – particularly those mechanisms that could be associated with embryonic or micro-crack formation, and these are discussed herein.

Keywords: electrical potential drop, EPD, ACPD, DCPD, creep, incipient damage, pressure vessels, P91, on-line monitoring, Type IV cracking

Introduction & background

The use of the electrical potential drop (EPD) technique for monitoring creep damage in specimens and plant components at high temperature has been demonstrated by the authors in both the online laboratory and semi-industrial contexts (1) as well as offline laboratory-based studies (2). The latter have been aimed at trying to understand the EPD changes seen (for both AC and DC regimes) during online monitoring. Both the online and offline studies were conducted on welded specimens, where the EPD was monitored across HAZ locations thought to be particularly susceptible to type IV cracking (and in both cases, in P91 steel).

In essence, EPD relies upon a measurement of a specimen's electrical impedance. In the case of direct currents, this translates specifically into the electrical resistance, but with alternating currents, capacitive and inductive components can join the electrical resistance to generate a more complex response [3]. Any changes in the path that an electrical current takes, can alter impedance. This is most readily seen in the case of direct currents where cracking leads to a constriction in the current path, a rise in resistance, and hence a rise in the measured potential drop required to deliver said current through the specimen. Other phenomena will alter resistance such as the appearance of cavities which again alter the current path.

Online monitoring, by its very nature, prevents a deep study of those gradual changes in the underlying microstructure that may well be responsible for the magnitude of the measured EPD, whilst studies on laboratory specimens suffer from signal variations due to the multi-specimen nature, loss of sensitivity, due to the interrupted testing and even loss of validity, given the often construed "ideal" laboratory conditions under which the measurements are made. On-line monitoring also has to make do with measuring an "average" EPD response over a fixed location, whereas off-line measurements can (with appropriate engineering) be undertaken as area-scans, or line-scans, which gauge the changes in EPD across and along a specimen – and so give spatial information (2).

Results emanating from the on-line study showed a consistent and reproducible, if subtle, rise in DC EPD (DCPD) values, almost all of the way through the lifetime of the specimens (of the order of a 5% rise over a lifetime of ca.10,000hrs) being tested (pressure vessels), and a commensurate drop in AC-EPD (ACPD). This was followed by rapid rises in both, just ahead of final fracture/rupture events. Laboratory testing on creep specimens revealed changes in absolute ACPD that were consistent with those seen in the on-line tests. By measuring EPD signal variations as "line-scans" taken by traversing across the HAZ of welds (with the specimens themselves actually being cut out of much larger welds), it was possible to detect peaks in the EPD, particularly ACPD. Peak heights, when plotted as normalised values, against remaining lifetime, revealed a trend which appeared to provide a means of gauging consumed life through ACPD measurements. As part of the latter study, other EM methods were employed in an attempt to find a reliable indicator of life fraction remaining, as well as more conventional methods such as replication and AFM (to try and ascribe the changes seen, to physical phenomena).

One of the conclusions of the off-line EPD study (2), was that the changes seen in the EPD signals were highly likely to be due to cavitation damage - there being a reasonable link between independent measurements that showed a rise in the density and size of cavities – and the changes seen in the DCPD. Cavitation would theoretically have an effect on the effective resistivity of a conductor (or more precisely, its resistance) simply through an effect linked to geometric changes in the cross-section available for conduction. However, it is difficult to see how changes in magnetic permeability and other EM parameters, as part of an independent and parallel study (4) could be ascribed to cavitation. Similarly, whilst a tentative link could be ascribed to the changes seen in the online DCPD results, explaining the reductions seen in on-line ACPD, in terms of cavitation appeared impossible. ACPD, and the linked EM measurements cited above (4), are more likely to be affected by the state of strain in a metal, and how this alters the shape and orientation of magnetic domains.

Given that the on-line changes seen were reproducible and the result of many separate experiments, this paper begins by making the assumption that DCPD (at least) was responding to cavitation. However, given the equation for the resistance of a conductor, a 5% rise in signal magnitude implies a 4.76% reduction in cross sectional area – a feat for which cavitation volumes, as routinely reported for P91 cannot fulfil (see later). Thus, a simplistic view of cavities reducing the area available for conduction is insufficient to explain the observed changes.

The development of cavities could, however, add to the path that electrons are required to take – and so raise the apparent resistivity, in essence lengthening the conductor in the cavitated zone via internal convolutions. Furthermore, the volume of actual metal (as

distinct from the volume calculated from external dimensions) will not alter in a creep test, however there may well be lateral strain in the direction of the tensile load. This could alter, although subtly, the aspect ratio of the conducting "portions" of the specimen and hence could, in theory, raise the resistance and hence the DCPD.

This paper attempts to bridge the gap between the studies already undertaken, and previously cited, by introducing a numerical model into the mix, which predicts the likely changes in EPD (specifically DCPD) on the assumption that these can be ascribed to certain known, and previously observed, microstructural changes. To begin with, cavitation is assumed as the determinant here, but as will be seen, the outcome of the modelling process, far from confirming the belief that cavitation is the issue, strongly hints at contributions from other factors.

Experimental and modelling

For accurate measurements on materials of good electrical conductivity, impedance is normally measured using a four-point arrangement of in-line electrical contacts, with the outer two connections delivering the excitation current, and the inner two allowing measurement of the potential drop, between these two inner connections, required to drive the excitation current through the specimen – this being directly related to the specimen's local impedance. Normally, crack-like defects act to raise the local impedance, and therefore can be detected by a rise in the local EPD. Measurements are usually simplified by ensuring that the excitation current is known and remains constant.

Meshing and modelling were carried out in COMSOL. The Joule heating subsection of the electromagnetic heating physics engine was used for all modelling in this study. This is because it gives a good approximation of the real-world scenario. The electric currents subsection of the AC/DC physics engine, could also have been used, but the extra work and computation time was deemed to be unnecessary. For ease, CAD modelling of the specimens and associated cavitation (porosity) was conducted in Fusion360 and imported it into COMSOL. This allowed a 4-point electrical connection to be modelled and then it was relatively easy to use the in-built "probe" facility to interrogate a specific boundary and extract a parameter from it, which in this case was calculated voltage.

Previous work should be consulted (2) in order to ascertain how close an approximation the modelled geometry was to that employed in laboratory testing – as well as to that encountered in the on-line monitoring studies (1), which showed the 5% rise in DCPD over the lifetime of the pressure vessels under test. The modelled system, although subtly different, was as close to "reality" as was deemed necessary, and any differences were regarded as unlikely to affect the validity of the results.

For the purposes of modelling, a similar specimen geometry to that used in the laboratory studies (2) was employed. This geometry, in turn, was as close as could reasonably be obtained to that present in the semi-industrial on-line tests cited earlier (1). Although the overall specimen size, during on-line testing, was an order of magnitude, or more, larger, the way in which the currents are injected into the specimen (real or virtual), and the location and spacing of the electrical contacts, makes it unlikely that significant differences in current flow would occur between the various testing scenarios. It is the current flow and distribution that ultimately determines the fundamental potential drops.

Initially a closer representation to the previously employed laboratory specimens was employed (see Figure.1a and b) but far faster processing times (of ca. 20 mins) were obtained by using a shorter specimen, with no significant alteration in the modelled current distribution and/or "measured" voltage. Figure 2 shows the base-line reference specimen that was eventually employed, and also details the parametric values chosen for the final models.

It should be noted that the previous off-line tests (2) using similar specimen geometries employed moving contacts (4 pin sprung-loaded probes) to deliver both the current and read back the resultant voltage, whereas the model presented here has fixed contacts – so is much more applicable to the on-line tests (1) which used spot welded connections onto the pressure vessels under test. Once again, the difference is not deemed likely to alter much in terms of measured values. The real purpose in the work was to ascertain whether cavitation is the likely driver for the DCPD signal changes previously observed.

The computational model defines the current injection at the top left of Fig 2, followed by a voltage (high) measurement point, a negative voltage (low) point, with the ground line (zero) line being at the current exit point at the lower right-hand side. The DCPD signal is the calculated differential voltage between the high and low voltage measurement points. For the purposes of modelling, a value of the metal's resistivity had to be set, and that for a high carbon steel was selected. Given that the current flow and distribution, in the DC case, is independent upon a material's resistivity (and only dependent upon specimen geometry and injection point) there was no need to obtain a precise value of the resistivity of P91 steel.

In addition to the reference, nine other models were created, each with different numbers of cavities (ranging from 2,000 to 16,000). The cavities were modelled as spheres and were located in the central zone of the specimen (between the voltage "contacts") in a volume of 5x5x10 mm (10 mm being the specimen width). This was regarded as representing the likely zone through which cavities could have extended over, in the previous experimental studies (1 & 2). All cavities were kept at 200 microns in diameter for the first batch of modelling.

Obtaining data on "real" creep cavities is not always straightforward as both reported dimensions and cavity numbers vary in the literature, and depend on the creep conditions and in particular on the materials chosen. Renversade et al (5) undertook an excellent study on cavitation in P91, and reported peak cavity sizes of around 2 microns in diameter for P91, and cavity densities of between 180k to over 700k per mm^3. These values proved too time consuming to model, and the decision was taken to raise cavity diameters to the point where modelling was feasible so as to ascertain, at the very least, whether the reported 5% change in DCPD could be attained via cavities alone.

To mesh the cavities, a 1x1 mm 2D grid of 16 squares was created in Fusion360 in the X-Y plane. Eight spheres were inserted in this grid in a regular hexagonal array. In effect, every other square in the array was populated with a sphere (thus generating 8 cavities). This was expanded into 3D by adding layers in the Z dimension, each rotated by 90 degrees with respect to the underlying layer. In total, 4 layers (each of 8 spheres) were generated and stacked together, as shown in Fig 3. This gave 32 spheres in total, in a 1 mm^3 volume. This was then replicated to generate an array of spheres in a 5x5x10 mm^3 volume followed by a Boolean subtraction to create a "cavitated" volume of the same

dimensions. Using this method, some 8000 cavities were evenly spaced in the 5x5x10 mm^3 volume.

To generate alternative cavity populations, it was necessary to either add cavities or remove them from this basic array of 8000. By filling every space in the original 16 square grid with a sphere, it was possible to reach a cavity population of 16,000. Values of 6000, 4000, 2000 (and 10,000, 12,000, 14,000) cavities were generated by sequentially removing spheres from the 8000-cavity array (or the 16,000 array respectively) in an orderly fashion. Spheres were removed sequentially such that large gaps did not develop in the array (for example, avoiding two empty grid squares adjacent to each other). This methodology was far simpler than attempting to re-arrange the spheres to ensure that the sphere spacing was kept uniform for each array. It is acknowledged that this methodology therefore generated arrays where the inter-sphere distances could vary across the array, but the effect on the current flow is likely to be a second order issue – and should therefore have a small influence on the modelled DCPD.

It is also acknowledged that the Boolean subtraction of cavities from the specimen is simplistic, and does not account for the fact that cavitation never removes material, it just reorganizes it. The Boolean operation here employed actually removes conductive material from the model, so would be expected to generate a rise in DCPD that would exceed that for a constant volume model. Thankfully, this discrepancy would be most noticeable and significant at high cavity volumes, rather than at the much lower cavity volumes observed by Renversade et al (5). With this in mind, the assumption was made that the drop in material solid volume, at low cavity volumes could be neglected, with the change in DCPD being assumed entirely to be due to the alteration in current path and the additional constraint of the current being funnelled between cavities.

Results and Analysis

A typical modelled current distribution is shown in Fig 4a. As expected, the flow is largely uniform away from the immediate area of the current contacts, but appears concentrated in the zone of the cavity array. Fig 4b is a close up of this area. The banding that can be seen is again as expected, given the cavity layers are effectively separated from each other by thin un-cavitated zones - -which are more conductive and hence show up as a lighter colour. The only way to eliminate this banding, would have been to somehow model an array of cavities where each layer partially encroached upon its nearest neighbours (much like the FCC crystal structure is generated by layers of atoms that partial interpenetrate each other. It is recognised that such an array is made up of high conductivity and lower conductivity layers – something unlikely in reality. For a given thickness of cavitated material, and contact separation, the model might be expected to return a slightly lower DCPD than if the layers interpenetrated, simply because the current path would be more convoluted.

The voltage outputs from each computed model are given in Table 1 together with the calculated values of total cavity volume (% porosity). Fig 5 plots the resultant DCPD against the % cavitation (porosity). The data is shown curve fitted to a 2^{nd} order polynomial, with the extrapolation forced through the origin. Percentage porosity was chosen as the representative parameter to plot, so as to assist extrapolation of the resultant response to the more representative data on cavity size, as obtained from the literature.

The data set shows that a 5% reduction in DCPD is easily demonstrated by the modelled array of cavities. By interpolation, a 5% change in DCPD would correspond to an approximate porosity of 12%, which equates to a little over 7000 cavities (of 200 micron diameter) in the 5x5x10 mm (250 mm^3) zone. Of course, as discussed in the introduction, the modelled cavity sizes are some 2 orders of magnitude larger than the ones observed by Renversade et al (5). Their study presented a typical cavity count for their sampled volumes of around $5x10^3$ cavities, but for 2 micron diameter cavities. Sampled volumes were estimated to be cylinders of 0.6 mm diameter and 25 micron thickness, giving a cavity density (ρ_c) of approximately $7.08x10^5$ cavities per mm^3. If these are assumed spherical, then each cavity has a total volume of $3.35x10^{-8}$ mm^3, and the total percentage porosity in our modelled zone of 5x5x10 mm is given by:

$$\%porosity = \frac{100(total\ pore\ volume)}{(sample\ volume)} = \frac{100(\rho_c V_s V_c)}{V_s} = 2.37\%$$

where V_c is the total volume of cavities, V_s is the cavitated-zone volume in the specimen and ρ_c is the cavity density (number per unit volume).

If this percentage porosity is substituted into the curve-fit data of Fig 5, an estimated percentage change in DCPD of 0.9% is generated. Whilst this is substantially lower than the 5% observed experimentally, it does provide support for some of the change seen in measured DCPD.

Whilst this analysis applies to the case of varying the cavity number, for a fixed cavity size (of 200 micron diameter), in order to check the validity of the modelling undertaken, further analysis was performed on arrays of cavities where the cavity size was altered, but the cavity number maintained constant. This was done to test the interchangeability of size with number, given that the experimentally observed cavities were very different in size from that modelled. Once again, the cavities were mathematically converted into a % porosity, and this was then plotted against the modelled DCPD. To expedite the modelling, an initial cavity radius of 200 microns was chosen, and a cavity number of 250. A series of 8 models were run with the cavity number being maintained at 250, and the cavity radius being increased in steps to 400 microns. This allowed a near 1:1 mapping of total porosity between the previous variable number model runs and these variable size runs thus permitting direct comparison of the plotted values.

A representative modelled current distribution is shown in Figure 6. This showed no noticeable difference, as expected, from the previous model runs where cavity number was varied. Conversion of the data to % porosity is given in Table 2, with the resultant plot of porosity against modelled DCPD given in Figure 7. The shape and rate of change of the curve-fit is almost identical to the previous plot (Figure 5), as are the curve fit coefficients. Substituting the calculated % porosity from Renversade (as given above) of 2.37%, gives an almost identical predicted change in DCPD of 0.89%.

Whilst this analysis relies upon an extrapolation to an effective pore size that is two orders of magnitude smaller than the smallest modelled, the close correspondence of both modelling approaches lends support that whatever parameter is altered, the modelled DCPD is primarily reliant on total percentage porosity (i.e. total cavity volume) rather than on the nuances of the morphology of the array of pores (which again seems a logical outcome).

The implications for the previous creep studies and changes in observed DCPD therein are significant, for whichever of the two modelling approaches is taken – in particular, the assumption that the DCPD is determined by cavity volume alone has now been shown to be flawed. The modelling approach taken here yields predicted DCPD changes that are only 20% of those seen in practice, if not smaller (given the large extrapolations that have been necessary in the modelled responses to attain "real" cavity volumes).

Whilst hitting a similar order of magnitude via the modelling is encouraging, it is clear that some modification to the initial thesis and assumptions may be required. A number of other factors could be at play here, which might conspire to raise the observed changes in DCPD fivefold. The modelling shows that there is a clear but highly subtle effect of cavitation morphology, (note the slight difference in curve-fit coefficients), so it is not entirely without merit to suggest that non-linear changes in morphology might have a more dramatic effect on modelled DCPD – for example, the possibility of cavities forming large local clusters, as creep proceeds - where the cavity volume might appear to grow predictably, but the cavity size and orientation might deliver a greater change in DCPD.

As highlighted earlier, the Boolean process employed in this work actually removed material, rather than reorganized it, and so cast some doubt on the validity of the modelling. In truth, a constant volume model would be expected to predict a lower change in DCPD, so the results obtained here might have been further muted if the model had been more refined.

Clearly the cavities will eventually coalesce and form larger cavities – but these are unlikely to be spherical (as assumed by the modelling) with the possibility of longer aspect ratio cavities forming locally. Eventually these cavities could take the form of embryonic cracks and thus the change in DCPD would be expected to take a different trajectory. Similarly micro-cracking has been extensively identified as a stage in creep damage development in P91 weldments, (e.g. (6)) so the experimental data may in fact be initially responding to cavitation, but then become dominated by cracks that develop through either cavity coalescence or micro-cracks developing from cavity arrays. Furthermore, it is likely that any coalesce of voids and the propagation of cracks be oriented perpendicular to the principal applied load, which in the work cited in both (1) and (2) was also be perpendicular to the line joining the current injection and voltage pick up points. In this respect, such defects will be expected to dramatically raise the measured DCPD, given the cracking directly interrupts the current flow by reducing the cross-sectional area for conduction. Similarly, any dilation in the specimen caused by localised strain in between cavities and cracks, will serve to further narrow and lengthen current paths, hence contributing to a rise in the DCPD, given that the resistance of a conductor is proportional to its length but inversely proportional to its cross-sectional area. This latter contribution, however, is expected to be orders of magnitude smaller than that due to a reduction in cross sectional area for conduction, (via the growth of the cavities and any microcracks), so could be negligible.

Overall, it seems that all the likely factors that are contributing to the resistance of the specimen are working in harmony to raise the resistance (and hence the potential drop), so the five-fold discrepancy we see between the model and the experimental measurements may not be so irreconcilable after all, and certainly could be explained, either in part or in full, by a refinement of the model to include micro-cracking as a contributory factor.

Conclusions

The work presented here has attempted to shed light upon some experimentally determined changes in DCPD seen in long term creep P91 specimens subjected to high temperatures. A simple model that centred on the postulate of an array of spherical cavities was able to show a modest rise in DCPD, but was not able to match the magnitudes of the experimentally determined rises. Modelled DCPD values were typically a fifth of the experimentally observed values but this failure should not be viewed too negatively, for both the nature of the model (simplified to aid timely computation) and the assumption that only cavitation is responsible for the changes seen, could be the reason for the discrepancies reported here. The possibility remains that other mechanisms are at play, which could further magnify up the measured DCPD – particularly those mechanisms that could be associated with embryonic or micro-crack formation.

From the literature, the development of micro-cracks during the lifetime of a creep specimen is attested, and the likely orientation of such cracks would be expected to be ideally placed to maximise the effect on the measured DCPD. It is possible, therefore, that as soon as practically measured DCPD values during a creep test exceed those predicted by the simple cavitation model, that the cavities have begun to coalesce and/or micro-cracks have begun to form. This suggests that DCPD could be used as a reliable indicator of the various stages occurring during creep damage development – certainly in the period before final rupture (whereupon the DCPD is observed to rise exponentially).

Acknowledgements

The authors would like to thank Dr D Allen, of ETD Consulting, for his helpful and perceptive advice and access to his years of experience of real-world creep cavitation.

References

1. Wojcik, A., Waitt, M., Santos, A. S., (2017), The use of the potential drop technique for creep damage monitoring and end of life warning for high temperature components. *Mater. High Temp. 34, pp.458–465*
2. Wojcik, A., Waitt, M., Santos, A. S., Shibli, A., (2021), Electrical Potential Drop for monitoring creep damage in high temperature plant
Mater. High Temp. 38(5), pp 330-341
3. Wojcik, A. G., (1995), Potential drop techniques for crack characterisation, *Materials World, 3(8) pp.379–381*
4. Wilson, W., Peyton, A., Allen, D., Shibli, A., Hasegawa, Y., (2020), The Development of an Electromagnetic (EM) Sensor Technique for Creep Damage
Detection and Assessment, *Proceedings of the MIMA Conference, ETD Ltd, enquiries@etd-consulting.com, Oct. 2020.*
5. Renversade, L., Ruoff, H., Maile, K., Sket, F., Borbély, A., (2014), Microtomographic assessment of damage in P91 and E911 steels after long-term creep, *Int. J. Mater. Res. (formerly Z. Metallkd.) 105(7), pp 622-627*
6. Abson, D. J., Rothwell, J. S., (2013) Review of type IV cracking of weldments in 9–12%Cr creep strength enhanced ferritic steels, *International Materials Reviews, 58(8), pp 437-473*

List of figures/figure captions

Figure 1. (a) LHS, a meshed CAD model of a representative creep test specimen, (b) RHS, the modelled current distribution. Note the current is input and extracted via the two large contact posts on the top surface, and the voltages "read" off on the inner two contact posts. The DCPD voltage is the differential signal between the two inner contacts. Modelling parameters are given alongside.

Figure 2. Simplified and shortened "reference" specimen showing identical modelled current flow. Modelling parameters are given alongside.

Figure 3. Cavity creation methodology, left to right a)

Figure 4. a) LHS, modelled current flow in a cavitated specimen, for a cavity size of 100 micron radius, and a cavity number of 8000, b) RHS, close up of the cavitated area showing the banding in the current flow, characteristic of the model and the way in which the cavities are stacked.

Table 1. Tabulated values of the modelled DCPD voltages and cavity volumes for a model that maintains cavity size at 100 micron radius, but with variable cavity count.

Figure 5. Plot of calculated DCPD against percentage total cavitation (% porosity) for the constant cavity radius (variable cavity count) model. Curve fit equation given on plot.

Figure 6. Modelled current flow in a cavitated specimen, for the constant cavity number model, but variable cavity size. 250 cavities are present, of 200 micron radius.

Table 2. Tabulated values of the modelled voltages and cavity volumes for a model that maintains count at 250, but with variable cavity radius.

Figure 7. Plot of calculated DCPD against percentage total cavitation (% porosity) for the constant cavity count (variable cavity radius) model. Curve fit equation given on plot.

Figures

Figure 1.

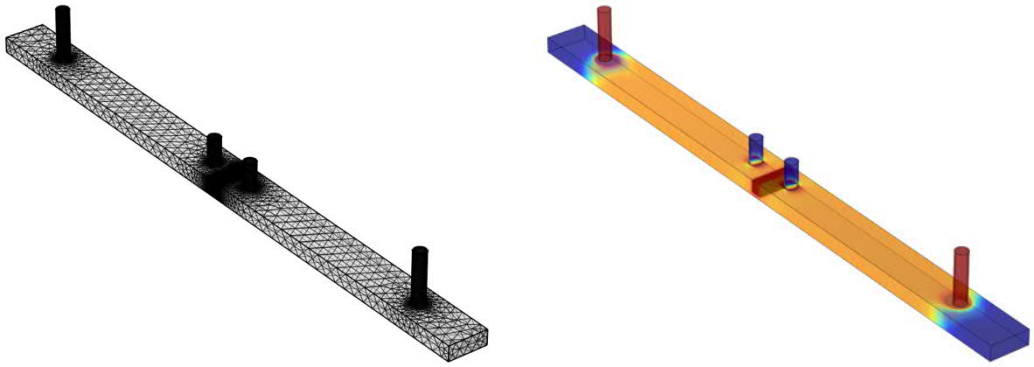

Model size: 250x16x6mm	Inward current density: 25mm from top edge
DC Current source: 2546479 A/m^2 Circa 50Amps	Positive contact: 90mm from inward current
Sphere size: 200micron diameter	Negative contact: 20mm from positive contact
Sphere number 12,000	Ground: 90mm from negative contact

Figure 2.

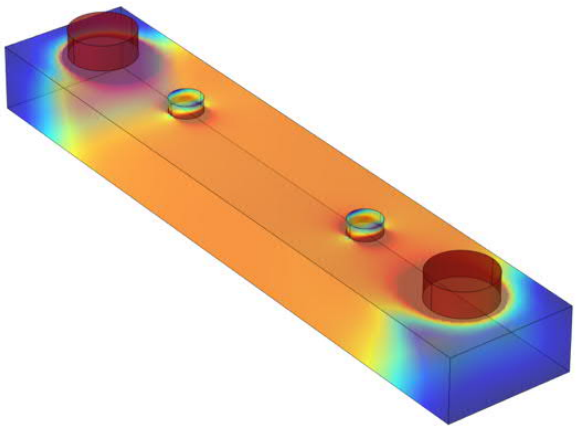

Model size: 50x10x5mm
Sphere size: None
Total volume of cavitation: None
DC Current source: 2546479 A/m^2, circa 50Amps
Inward current density: 5mm from the top edge
Voltage high contact: 10mm from inward current
Voltage low contact: 20mm from positive contact
Ground: 10mm from negative contact
High contact voltage: 0.0079374V (modelled)
Low contact voltage: 0.0029944V (modelled)
Differential voltage: 0.0049430V

Figure 3.

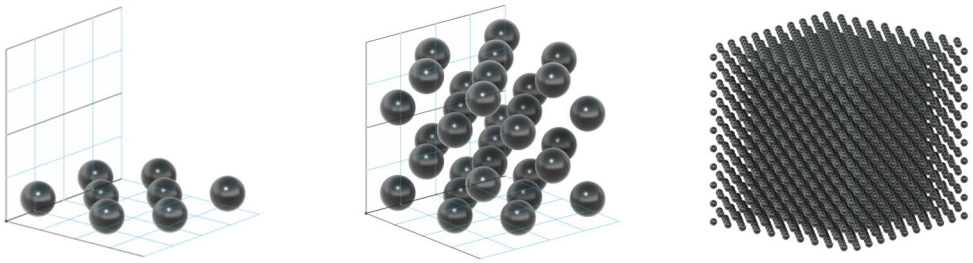

Figure 4.

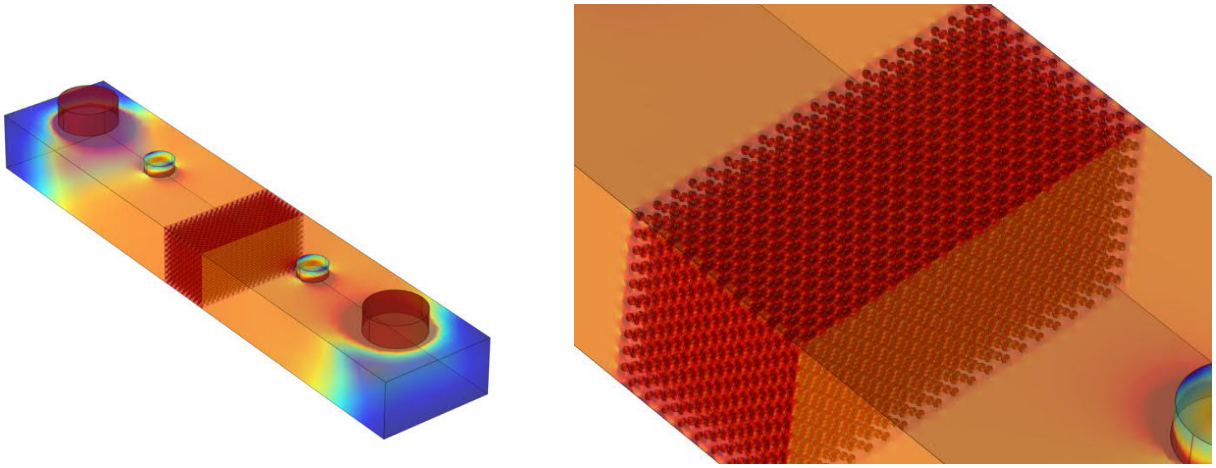

Model size: 50x10x5mm	Voltage low contact: 20mm from positive contact
Sphere size: 200micron diameter X8000	Ground: 10mm from negative contact
Total volume of cavitation: 33.51032mm^3	Voltage high (modelled) voltage: 0.0082002V
DC Current source: 2546479 A/m^2 circa 50Amps	Voltage low (modelled) voltage: 0.0029766V
Inward current density: 5mm from top edge	Differential voltage: 0.0052236V
Voltage high contact: 10mm from inward current	

Table 1

Cavity radius (mm)	Single cavity vol (mm^3)	Total cavity vol (mm^3)	Calculated % change in DCPD	Calculated % porosity of test vol
0	0	0	0	0
0.2	0.03351	8.37758	1.298806	3.351032
0.251984	0.067021	16.75516	2.700789	6.702064
0.28845	0.100531	25.13274	4.205948	10.0531
0.31748	0.134041	33.51032	5.83249	13.40413
0.341995	0.167552	41.88791	7.596601	16.75516
0.363424	0.201062	50.26547	9.522557	20.10619
0.382586	0.234572	58.64305	11.62654	23.45722
0.4	0.268083	67.02064	13.95913	26.80826

Figure 5.

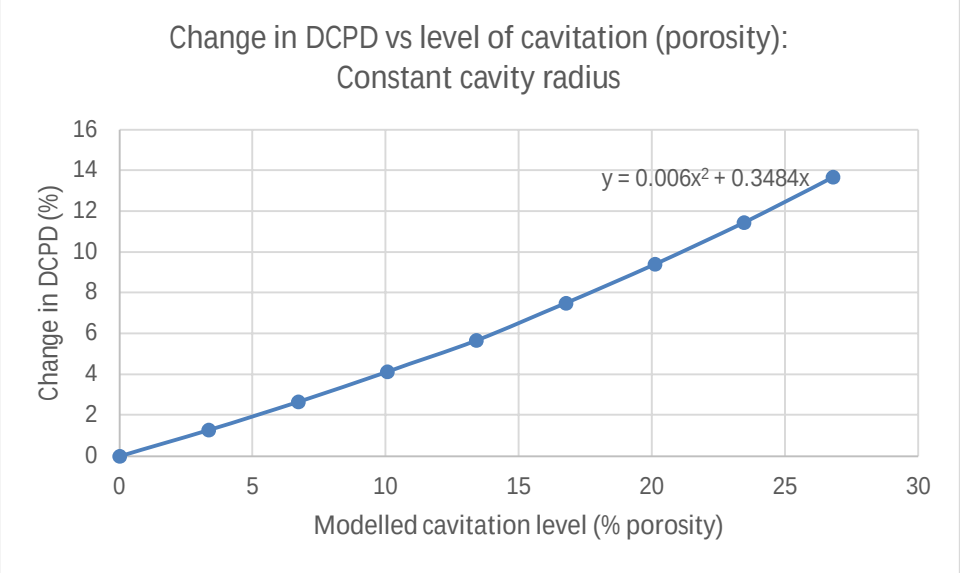

Figure 6.

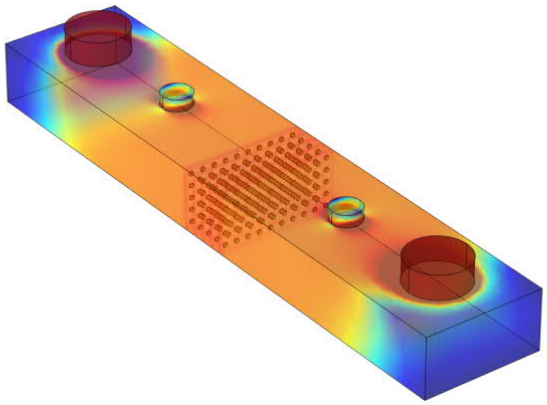

Model size: 50x10x5mm
Sphere size: 400micron diameter X250
Volume of each cavity: 0.033510mm^3
Total volume of cavitation:8.37758041 mm^3
DC Current source: 2546479 A/m^2, circa 50Amps
Inward current density: 5mm from top edge
Voltage high contact: 10mm from inward current
Voltage low contact: 20mm from positive contact
Ground: 10mm from negative contact
High contact voltage: 0.0079983V (modelled)
Low contact voltage: 0.0029911V (modelled)
Differential voltage: 0.0050072V

Table 2

Number of cavities	Single cavity vol (mm^3)	Total cavity vol (mm^3)	Calculated % change in DCPD	Calculated % porosity of test vol
0	0.004189	0	0	0
2000	0.004189	8.37758	1.278576	3.351032
4000	0.004189	16.75516	2.656282	6.702064
6000	0.004189	25.13274	4.147279	10.0531
8000	0.004189	33.51032	5.676715	13.40413
10000	0.004189	41.8879	7.50354	16.75516
12000	0.004189	50.26548	9.40522	20.10619
14000	0.004189	58.64306	11.45661	23.45723
16000	0.004189	67.02064	13.66579	26.80826

Figure 7.

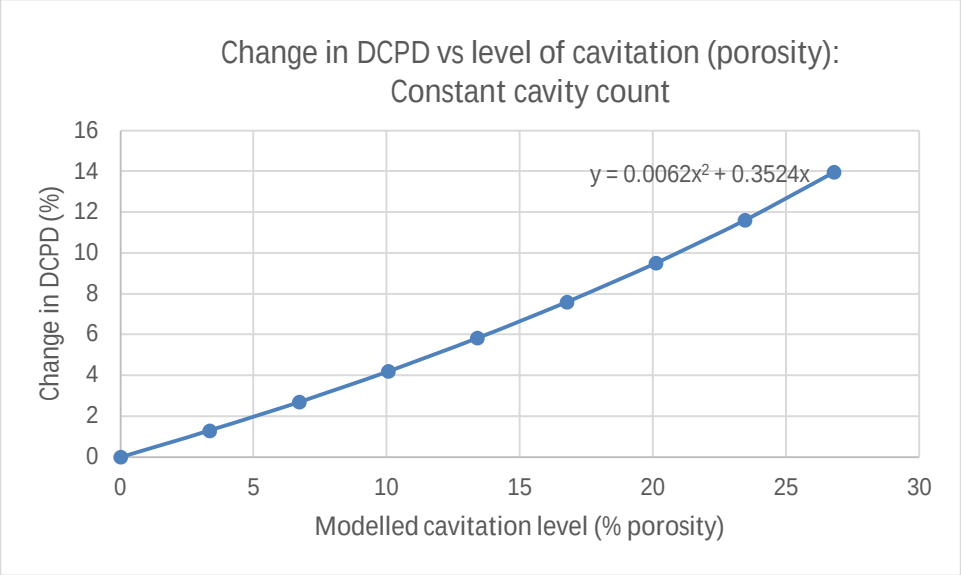

End of manuscript